Received October 26, 2018, accepted November 11, 2018, date of publication November 23, 2018,
date of current version December 18, 2018.

Digital Object Identifier 10.1109/ACCESS.2018.2883097

A Miniaturized and High Gain Double-Slot Vivaldi Antenna Using Wideband Index-Near-Zero Metasurface

SHUANGSHUANG ZHU[1], (Student Member, IEEE), HAIWEN LIU[1], (Senior Member, IEEE), PIN WEN[1], (Student Member, IEEE), LIXIA DU[2], AND JIAFENG ZHOU[3]

[1]School of Electronic and Information Engineering, Xi'an Jiaotong University, Xi'an 710049, China
[2]School of Electronic of Engineering, East China Jiaotong University, Nanchang 330013, China
[3]Department of Electrical Engineering and Electronics, University of Liverpool, Liverpool L69 3GJ, U.K.

Corresponding author: Haiwen Liu (haiwen_liu@hotmail.com)

This work was supported in part by the National Natural Science Foundation of China under Grants U1831201 and Grant 61728106, in part by the Natural Science Foundation of Jiangxi Province of China under Grant 2017ACB20019, in part by the Science & Technology 5511 Project and Research Program of Jiangxi Province of China under Grants 2016BCB18010 and 20171BBE50056, and in part by the Young Science Foundation of Jiangxi Province of China under Grant 20171BAB212001.

ABSTRACT In this paper, a wideband, miniaturized, and high gain double-slot Vivaldi antenna is proposed. First, a corner cutting technique is adopted to broaden the frequency band. Second, a pair of defected ground slots is added to the edges of the antenna to extend the low-end frequency limitation from 2.27 to 1.15 GHz, which provides a great design freedom. Third, a novel unit cell of an index-near-zero metasurface is proposed in our design. The unit cell is a two-stub-loaded split-ring resonator, which has a compact size, a wide frequency band, and a good reflection coefficient. The gain of the double-slot Vivaldi antenna is improved over a wide frequency band by the inclusion of the index-near-zero metasurface in the aperture, without changing the overall dimensions or compromising the whole frequency band performance of the antenna. Finally, to verify the design method, an ultra-wideband double-slot Vivaldi antenna with defected ground slots and metasurface was fabricated and measured. The circuit has an overall size of 0.76 $\lambda g \times 0.41\ \lambda g \times 0.005\ \lambda g$. The modified antenna exhibits a measured gain of 0.7–14 dBi over the frequency band of 1.13–12 GHz.

INDEX TERMS Defected ground slot, high gain, index-near-zero, metasurface, Vivaldi antenna.

I. INTRODUCTION

A tapered slot antenna with exponential profile, namely Vivaldi antenna, was first introduced by Gibson in 1979 [1]. It is attractive because of its features of wide bandwidth, low profile, easy fabrication, and low cost. It is widely used in many applications, such as early-stage cancer detection [2], through-wall multiple targets detection [3], microwave interferometric radiometry [4], and concealed weapon detection [5]. Nowadays, extension of impedance bandwidth, size reduction, and radiation characteristics improvement of Vivaldi antennas simultaneously are still challenging in practical applications. Stripline right-angle bend with slant-wise corner cut [6], a stepped connection structure [7], and a tapered transition [8] were employed to improve impedance bandwidth. In order to ensure that the standing wave energy of Vivaldi antenna can be effectively radiated from the slot, the aperture width is suggested to be no less than a half-wavelength of the operated lowest frequency in free space when Vivaldi antenna designed [1], especially very long in the tapering direction [9]. Thus, various techniques have been developed to miniaturize Vivaldi antennas by using bending feed line structure [10], loading structures [11], or applying tapered slot edges [12].

However, these structures have low gains and more detailed comparison is shown in Section III. In recent articles, several researchers have proposed methods to enhance the gain of Vivaldi antennas, including the use of dielectric lens [13], higher dielectric constant slab [14], and parasitic patch [15] in the flared aperture section to guide energy in the endfire direction. Whereas, all these methods improve the performance at the expense of fabrication complexity or a large size. Therefore, it is still a great challenge to optimize the design and performance of a Vivaldi antenna to achieve high gain with a relatively small size.

Recently, the application of metamaterial structure to antenna design has been investigated widely along with the development of metamaterials [16]. In contrast to previous index-near-zero metamaterial, antenna in which the metamaterial was used to enhance antenna bandwidth [17], index-near-zero metamaterial could also be employed to achieve high directive emission of electromagnetic (EM) waves [18]. Some effective Vivaldi antenna structures with metamaterials were reported recently in [19] and [20]. In addition, a double-slot Vivaldi antenna (DSVA) was proposed [21], whose gain is higher than a conventional Vivaldi antenna with same size. However, the related researches or theoretical analysis in DSVA with metamaterial are rarely reported and analyzed [22].

In this paper, a miniaturized DSVA with high gain is proposed. The broadening of bandwidth miniaturization of size and improvement of gain are investigated and realized. A step-by-step design procedure is described in detail, which includes: 1) broadening antenna bandwidth by using a corner cutting technique [23], [24] to improve the impedance matching of a T-junction power divider; 2) extending the low-end frequency limitation by etching a pair of defected ground slots on the radiation surface of the DSVA; 3) enhancing the gain of the DSVA by adding a novel compact index-near-zero metasurface (MS) – a planar metamaterial. Finally, the modified DSVA is fabricated and measured to verify the proposed design.

II. DESIGN AND ANALYSIS OF THE DSVAs

The DSVA of T-junction power divider with corner cutting (named Ant I) design follows the concept described in [21], which is shown in Fig. 1(a). The DSVA makes the aperture field distribution at the end of the antenna more uniform, thus the gain of the proposed antenna is higher than that of a conventional Vivaldi antenna with the same size.

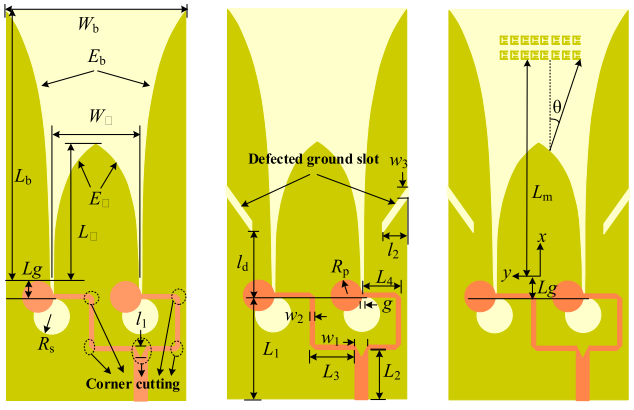

FIGURE 1. Configurations of (a) Ant I: T-junction power divider with corner cutting, (b) Ant II: Ant I with a pair of defected ground slots, and (c) Ant III: Ant II with the proposed MS. The geometrical dimensions are $L_a = 60$, $L_b = 120$, $L_1 = 25$, $L_2 = 13$, $L_3 = 18.995$, $L_4 = 10.15$, $Lg = 5$, $L_m = 97$ mm, $W_a = 40$, $W_b = 80$, $R_p = 3.5$, $R_s = 4$, $l_1 = 2.7$, $l_2 = 16$, $l_d = 27$, $w_1 = 2.78$, $w_2 = 0.77$, $w_3 = 0.5$, $g = 0.3$ (all in mm).

The Ant I contains two metal layers: tapered slot and microstrip power divider are printed on the top and bottom layer, respectively. A Wang Ling F4BM265 substrate, whose thickness, permittivity and loss tangent are 1 mm, 2.65, and ≤ 0.001, respectively, is used as the middle layer. The exponentially tapered slot profiles E_a and E_b can be described by [1]:

$$E_a : y = \pm 0.5(W_a - g \times \exp(\frac{x\mathrm{In}(W_a/g)}{L_a}) \quad (1)$$

$$E_b : y = \pm 0.5(W_a - g \times \exp(\frac{x\mathrm{In}((W_b - W_a)/g)}{L_b}) \quad (2)$$

The overall size of Ant I is 130 mm × 80 mm × 1 mm.

In order to improve the impedance matching of DSVA, corner cutting is added to the microstrip power divider. A T-junction power divider with corner cutting can be equivalent to a two-port network. A good matching network to eliminate the reflected power can be obtained through designing suitable corner cutting. To study the characteristics of impedance matching, the input impedance is obtained by simulating with variable l_1 and w_1. In Fig. 2, it can be seen that the optimized input impedance matching characteristics of Ant I can be obtained by choosing appropriate l_1 and w_1. Its S_{11} is presented in Fig. 3, where a good impedance

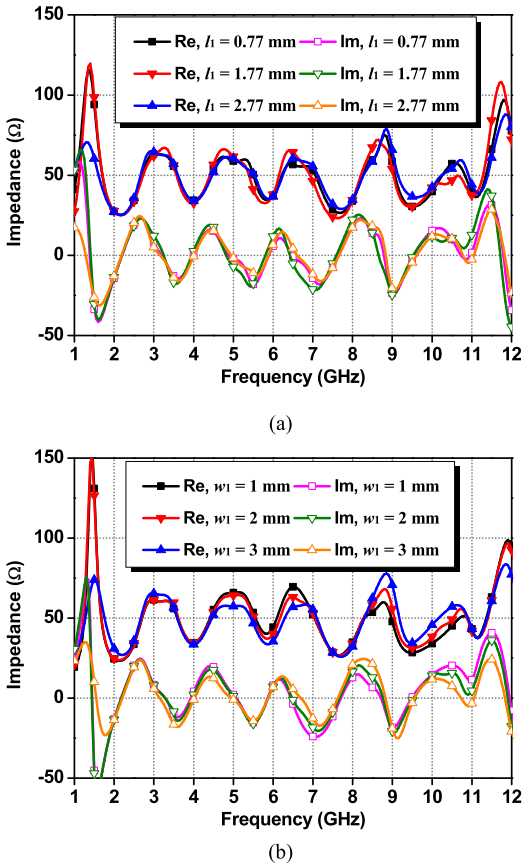

FIGURE 2. Input impedance of Ant I as a function of (a) l_1 and (b) w_1.

matching can be observed in a wide frequency band of 2.27–12 GHz.

A. MINIATURIZED DSVA DESIGN

Vivaldi antenna at the frequencies that lower than the low cut-off frequency have edge diffraction and cannot work. To further achieve miniaturization, the increasing edge diffraction path through adding circular-shape-patch [11], [25], and many slots [12], [13] was used to reduce the low cut-off frequency of Vivaldi antenna. In this section, a pair of defected ground slots are etched on the radiation surface of Ant I and Ant II is presented in Fig. 1(b). The S_{11} of Ant II is also demonstrated in Fig. 3. It has a fractional bandwidth of 165% from 1.15 up to 12 GHz. To further understand the effectiveness of the defected ground slots on extending the low frequency band end, surface current distributions of Ant I and Ant II at 1.15 GHz are shown in Fig. 4. Ant I has relatively intense current in region "R_1" at the edges of radiators while Ant II has intense current in region "R_2." The effective electrical length of the current path on Ant II is increased, result in extending the low frequency band end from 2.27 GHz to 1.15 GHz.

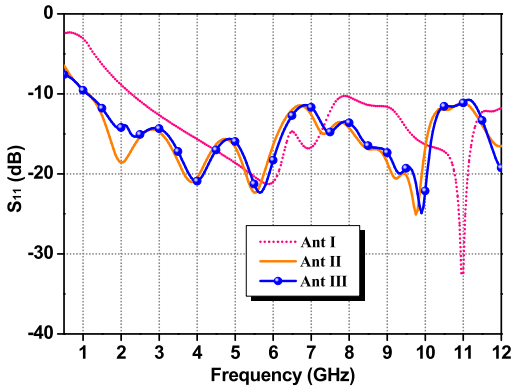

FIGURE 3. Comparison of simulated S_{11} for Ant I, Ant II, and Ant III.

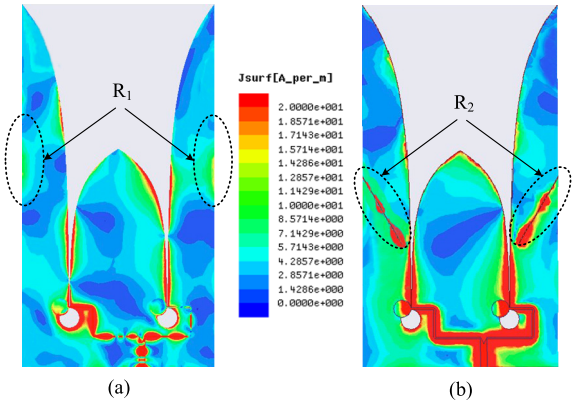

FIGURE 4. Surface current distributions of (a) Ant I and (b) Ant II at 1.15 GHz.

Numerical studies on the defected ground slots positions (l_d) and dimensions (l_2 and w_3) have been performed and

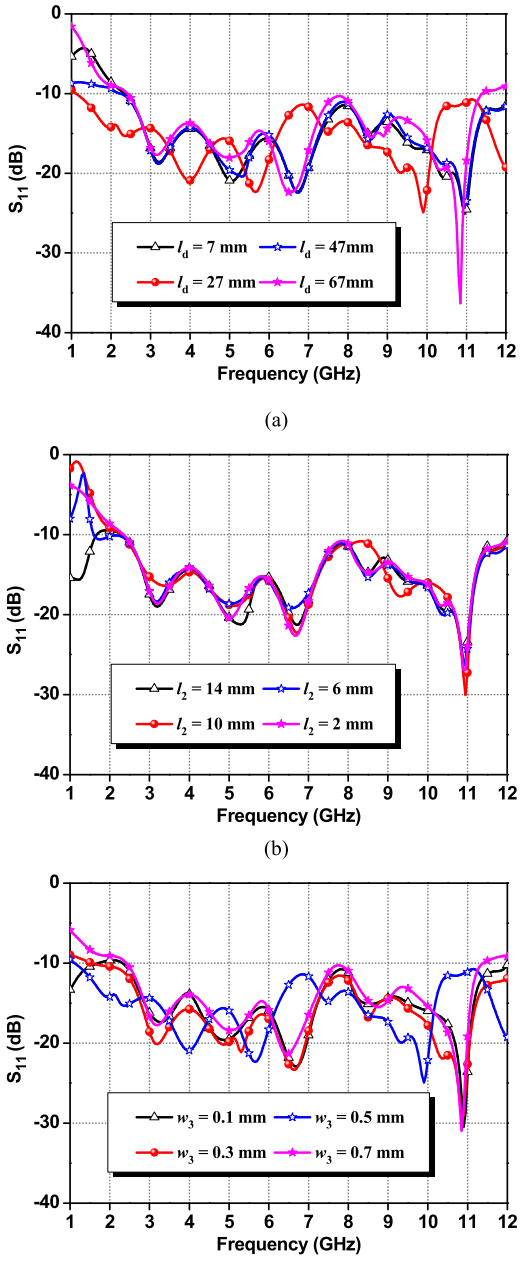

FIGURE 5. Simulated S_{11} of Ant II with variables (a) l_d, (b) l_2 and (c) w_3.

shown in Fig. 5. It is found that l_d and w_3 mainly affects the lower frequency band and the upper frequency band. The influence of l_2 on the whole frequency band is not obvious. Thus, the defected ground slots can be adopted to reduce the low cut-off frequency.

The gain of Ant II versus the operating frequency is shown in Fig. 6. Within the frequency range of 1.15–12 GHz, the minimum gain is 1.11 dBi at 1.15 GHz and the maximum gain is 14.46 dBi at 10.5 GHz. Whereas the gain of Ant I is 3.62–14.2 dBi in the frequency band of 2.27–12 GHz. The gain of Ant I at low frequency band of 1.15–2.27 GHz is significantly lower than that of Ant II, which further verify that Ant II can achieve miniaturization compared to Ant I.

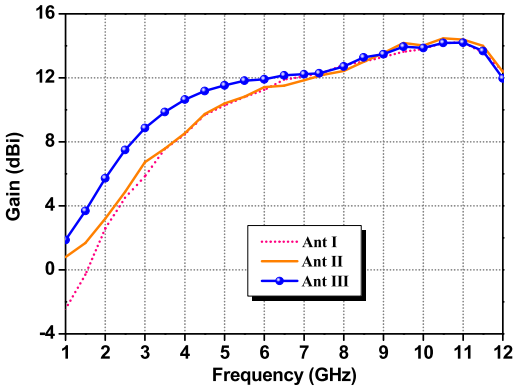

FIGURE 6. Comparison of simulated gains for Ant I, Ant II, and Ant III.

B. DSVA WITH HIGH GAIN DESIGN

Fig. 7 presents the E-field distributions of Ant II at 1.15 GHz, 5 GHz, 8 GHz, and 12 GHz. It is noted that the aperture field distribution of Ant II at low frequency is nonuniform, which leads to the gain decreases. According to the literature [19], [20], an MS can be used to increase the gain of directional antennas. To design a high gain Vivaldi antenna based on MS, the first step is to find a proper element that is non-resonant at the desired frequency band. As is shown in Fig. 8(a), the proposed unit cell of MS is a two-stub-loaded split-ring resonator (SRR) printed on a same F4BM265 substrate as the one used in the Vivaldi antenna design. This structure can be easily integrated within a planar Vivaldi antenna due to its compact design.

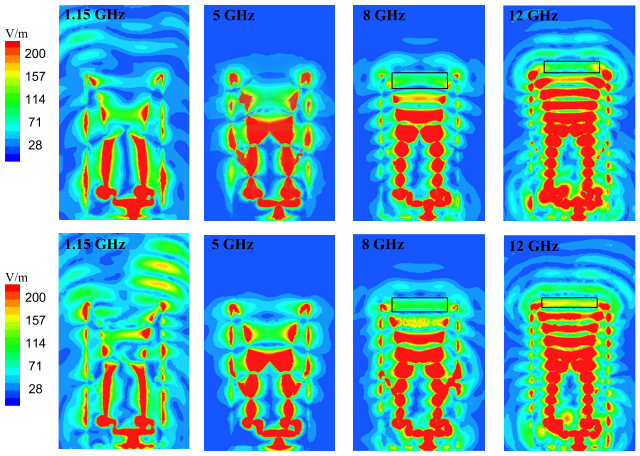

FIGURE 7. Comparison of E-field distributions for Ant II (upper) and Ant III (lower) at 1.15 GHz, 5 GHz, 8 GHz, and 12 GHz. (a black solid line rectangle is given in each graph at 8 GHz and 12 GHz)

The characterizations of the entire MS can be reduced to that of a single unit cell as a result of the periodicity, as shown in Fig. 8(b). The unit cell is excited by a plane wave, and four sides of the structure are set as perfect electric conductor (PEC) and perfect magnetic conductor (PMC) boundary conditions, respectively. The electric polarization of the EM wave is along the y-axis. The transmission characteristics of

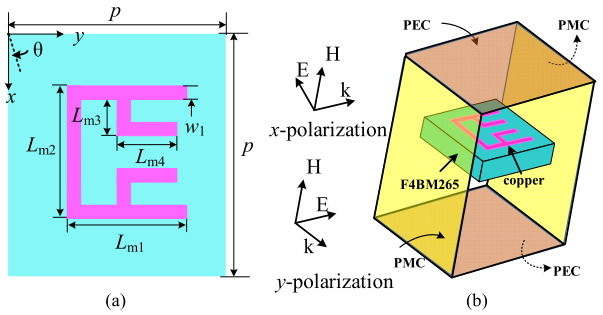

FIGURE 8. (a) Configuration of the proposed metasurface element and (b) its simulation model at y-polarization. The geometrical dimensions are $L_{m1} = L_{m2} = 2$, $L_{m3} = 0.6$, $L_{m4} = 1$, $p = 4$, $w_1 = 0.2$ (all in mm). The buff planes in (b) represent perfect electric conductor (PEC) and the deep orange planes represent perfect magnetic conductor (PMC).

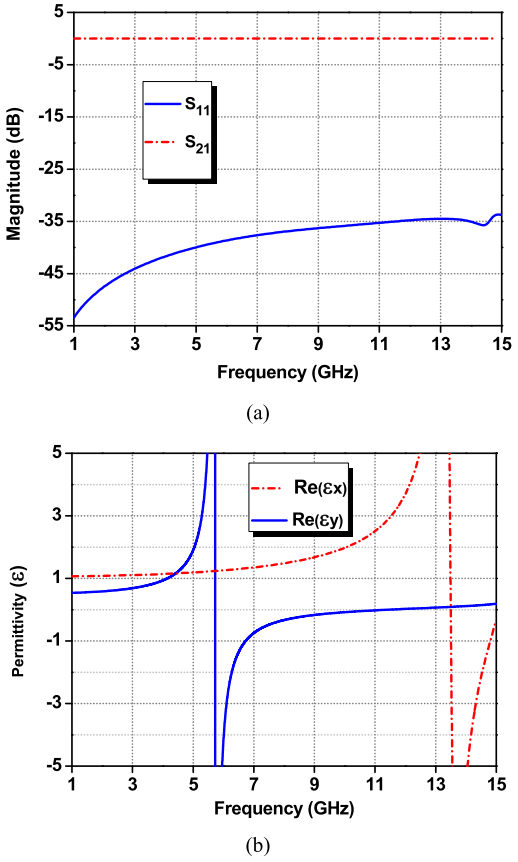

FIGURE 9. (a) The S parameters, and (b) retrieved permittivity of the proposed MS at x-polarization and y-polarization.

the designed MS are demonstrated in Fig. 9(a). As shown in this figure, the S_{11} is better than –10 dB over the frequency range of 1–12 GHz, which ensures that most of the radiation power of the Vivaldi antenna can be transmitted through the MS within the wide frequency band. The extracted real part of the permittivity (ε_y) of the proposed MS are shown in Fig. 9(b), according to the formulas provided in [26]. It is shown that the zero index point is observed in the frequency band. Besides, the electric polarization of the EM wave along the x-axis are also given and the characteristic

TABLE 1. Comparison between the proposed metasurface and others.

Ref.	Frequency band of Vivaldi antenna (GHz)	S_{11} of the metasurface	Unit cell size ($\lambda_g \times \lambda_g$)
[19]	1–15	NA	0.017 × 0.012
[20]	57–66	–10 dB ~ –5 dB	0.293× 0.24
[27]	2–12	–20 dB ~ –6 dB	0.035 × 0.033
This work	**1–12**	**–54 dB ~ –35 dB**	**0.009 × 0.009**

λ_g is the guided wavelength at the lowest frequency of the resonant band.

is used for comparison. The extracted real part of permittivity (ε_x) is always bigger than zero in the frequency band of 1–12 GHz, which is not suitable for designing to improve antenna gain. Thus, the *y*-polarization of the MS is chosen in the antenna design. Table 1 compares the proposed MS with other reported metamaterials, which were used in Vivaldi antenna designs to improve the directivity. It demonstrates the superiority of the S_{11} and unit size of the proposed MS. One is that S_{11} of the proposed metasurface is better, which is added to slot of the Vivaldi antenna and has little influence on the original radiation of the Vivaldi antenna. The other is that the unit size the proposed metasurface is smaller, thus more unit cell structures can be added in the same amount of space, which improve design freedom and accuracy. Therefore, the proposed MS has significant advantage in designing the Vivaldi antenna with low loss.

In order to improve the gain in a wide frequency band, the aforementioned two-stub-loaded SRRs are added to the slot of Ant II. It is no longer necessary to place the MS at a reasonable distance from Antenna [22], and hence a low profile and high gain Ant II with MS (Ant III) can be achieved in this case, as demonstrated in Fig. 1(c). Fig. 3 shows the S_{11} of Ant III, which is less than –10 dB from 1.11 to 12 GHz. It demonstrates that the proposed MS does not deteriorate the impedance bandwidth of Ant II as expected. The gain of Ant III versus frequency is shown in Fig. 6, with the gain of Ant II as a reference. Ant III can achieve an obviously larger gain at frequencies below 6 GHz. And the gain of Ant III is maximum increased by 2.28 dB at 3.5 GHz compared to Ant II.

Subwavelength structure that unit cell is smaller than the wavelength has some characteristics such as refractive index manipulation [28]. The phenomenon of gain enhancement caused by the designed MS can be interpreted by the refractive law. The extracted real and imaginary parts of the refractive index (n) of the designed MS are shown in Fig. 10, according to the formulas provided in [26]. It is demonstrates that the zero index point is observed in the frequency band and the region of $|\mathrm{re}(n)| < 1$ is located in a wide frequency range at the oblique incidence, where θ is the angle between the incident wave and the x-axis, as shown in Fig. 8(a). Thus, the proposed MS has the performance of converging the EM wave in a wide frequency band.

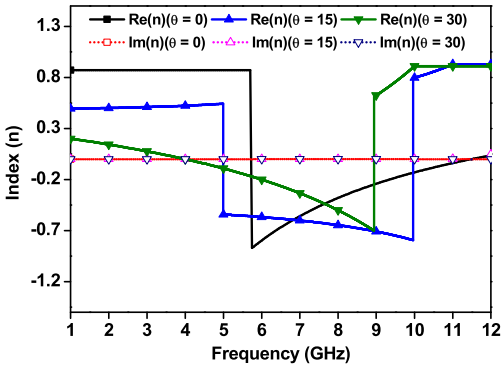

FIGURE 10. The retrieved refractive index of the proposed MS at different incident angles. θ represents the angle between the incident wave and the *x*-axis.

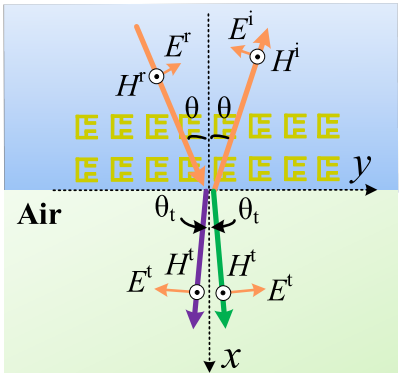

FIGURE 11. Wave incident on the interface of the MS and air (purple refracted ray: re(*n*) < 0, green refracted ray: re(*n*) > 0, n is the refractive index of the MS).

In order to verify the convergence performance, Fig. 11 shows the propagation of an EM wave with an oblique incident angle. The boundary plane is the $x = 0$ plane and the incident plane is the xy-plane. The incident electric field E^{i}, reflected electric field E^{r}, and transmitted electric field E^{t} are defined as

$$E^{\mathrm{i}} = E_0^{\mathrm{i}} e^{-jk_1(x\cos\alpha_{\mathrm{i}} + y\cos\beta_{\mathrm{i}})} \tag{3}$$

$$E^{\mathrm{r}} = E_0^{\mathrm{r}} e^{-jk_1(x\cos\alpha_{\mathrm{r}} + y\cos\beta_{\mathrm{r}} + z\cos\gamma_{\mathrm{r}})} \tag{4}$$

$$E^{\mathrm{t}} = E_0^{\mathrm{t}} e^{-jk_2(x\cos\alpha_{\mathrm{t}} + y\cos\beta_{\mathrm{t}} + z\cos\gamma_{\mathrm{t}})} \tag{5}$$

where k_1 and k_2 are the propagation constants of the MS and air, respectively. α_{i}, β_{i}, γ_{i} are the angles between the incident wave and the x-, y-, z-axes, respectively. α_{r}, β_{r}, γ_{r} are the angles between the reflected wave and the x-, y-, z-axes, respectively. α_{t}, β_{t}, γ_{t} are the angles between the transmitted wave and the x-, y-, z-axes, respectively. E_0^{i}, E_0^{r}, E_0^{t} are the amplitudes of the incident, reflected, and transmitted electric fields, respectively. The relationship among the incident electric field, reflected electric field, and transmitted electric field can be found according to the boundary condition theory that the tangential components of electric fields must be continuous:

$$\left[E_0^{\mathrm{i}} e^{-jk_1 y\cos\beta_{\mathrm{i}}} + E_0^{\mathrm{r}} e^{-jk_1(y\cos\beta_{\mathrm{r}} + z\cos\gamma_{\mathrm{r}})}\right]_{\mathrm{t}} = \left[E_0^{\mathrm{t}} e^{-jk_2(y\cos\beta_{\mathrm{t}} + z\cos\gamma_{\mathrm{t}})}\right]_{\mathrm{t}} \tag{6}$$

Equation (6) can be applied to any x and y variables, thus,

$$0 = k_1 \cos \gamma_r = k_2 \cos \gamma_t \tag{7}$$

$$k_1 \cos \beta_i = k_1 \cos \beta_r = k_2 \cos \beta_t \tag{8}$$

According to (7), it can be found

$$\cos \gamma_r = \cos \gamma_t = 0 \tag{9}$$

which means that

$$\gamma_r = \gamma_t = \pi/2 \tag{10}$$

Both the reflected ray and the transmitted ray are located on the xy-plane. In addition, according to Fig. 11 it can be seen that:

$$\beta_i = \frac{\pi}{2} - \theta, \quad \beta_r = \frac{\pi}{2} - \theta, \quad \beta_t = \frac{\pi}{2} - \theta_t \tag{11}$$

From (8) and (11) we can get the Snell's Refraction Law

$$\sin \theta_t / \sin \theta = k_1/k_2 = \mathrm{re}(n)/\mathrm{re}(n_2) \tag{12}$$

where n and n_2 are the refraction index of the MS and air, respectively.

To illustrate how this property can help control the propagation of a wave, an incident wave on the interface with an oblique angle is considered. Equation (12) implies that with an index-near-zero and $|\mathrm{re}(n)| < 1$ the ray in the air will be refracted in a direction very close to the normal. Then, all the refracted rays will be in almost the same direction as demonstrated in Fig. 11. Thus the gain will be increased, as shown in Fig. 6. The E-field distributions of Ant III at 1.15 GHz, 5 GHz, 8 GHz, and 12 GHz are presented in Fig. 7. It can be clearly seen that the aperture field distributions of Ant III are more uniform than that of Ant II at lower frequencies (1.15 GHz and 5 GHz), which contributes to the gain improvement of Ant III. At higher frequencies (8 GHz and 12 GHz), the aperture fields of Ant II are already close to a plane-like wavefront, and the phase delays of metasurface at higher frequencies are small. Thus, the effect of phase compensation at higher frequencies is weak after adding the metasurface. However, the proposed MS introduces more metal losses at higher frequencies. Though the aperture field distributions of Ant III are more uniform than that of Ant II at higher frequencies, metal loss introduced by the proposed MS will contributes to gain decrease. As a result, the gain of Ant III is approximate to that of Ant II at higher frequencies, as shown in Fig. 6. Thus, the number of MS 2×8 is used in the final antenna design.

Furthermore, the phase distribution mechanism can also be used to analyze the gain improvement. Recent investigation revealed that aperture electric fields of directional antennas have nonuniform phase distribution, which reduces the effective radiation and results in a lower peak directivity [29]. Therefore, metamaterial, which has a phase delay when an EM wave transmits through it, can be designed as a phase compensator to reduce the nonuniformity of phase distribution.

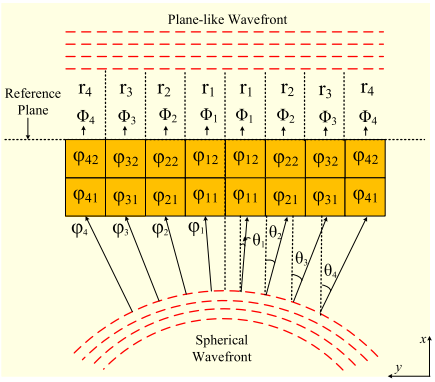

FIGURE 12. Path diagram of MS converts a spherical wavefront into a plane-like wavefront. θ_n represent the angle between the radiation direction of the proposed Ant III and the x-axis.

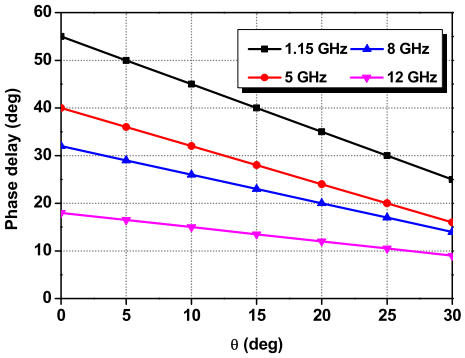

FIGURE 13. Phase delays of the designed MS versus incident angle at 1.15 GHz, 5 GHz, 8 GHz, and 12 GHz.

Fig. 12 illustrates that how a MS converts the spherical wavefront radiated by a Vivaldi antenna into a plane-like wavefront. The rays pass through the edge will incur more delay than those pass through the center of a Vivaldi antenna. Thus, the nearly uniform phase distribution can be obtained by adding more delay in the center of a Vivaldi antenna. The phase at the aperture plane of Ant III is denoted by φ_n and the desired out-plane phase from MS is denoted by Φ_n. Thus,

$$\Phi_1 = \varphi_1 + \varphi_{11} + \varphi_{12} \tag{13}$$

$$\Phi_n = \varphi_n + \varphi_{n1} + \varphi_{n2} \tag{14}$$

where φ_{n1} and φ_{n2} represent the phase delays of MS unit cell. In order to convert the spherical wavefront radiated by a Vivaldi antenna into a plane-like wavefront, the phase at the reference plane should be equal:

$$\Phi_1 = \Phi_2 = \cdots\cdots = \Phi_n \tag{15}$$

that is

$$\varphi_1 + \varphi_{11} + \varphi_{12} = \varphi_2 + \varphi_{21} + \varphi_{22} = \cdots\cdots = \varphi_n + \varphi_{n1} + \varphi_{n2} \tag{16}$$

In this work, we consider the phase delay value of the proposed MS in different incident angles. Fig. 13 shows the phase delay information at 1.15 GHz, 5 GHz, 8 GHz,

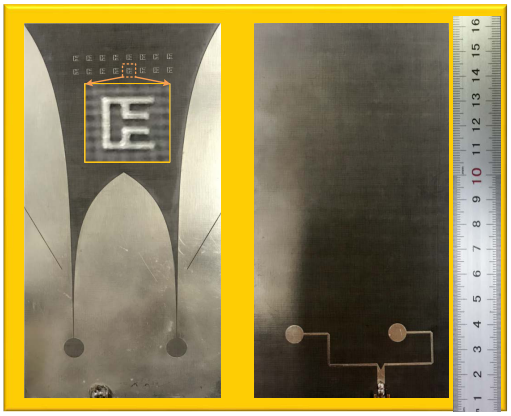

FIGURE 14. Fabricated prototypes of the proposed Ant III (left) top view and (right) bottom view.

and 12 GHz versus incident angle. As the incident angle increases–the position of the MS is closer to the edge of Vivaldi antenna–the phase delay decreases, which satisfy the center of a Vivaldi antenna needs more phase delay and the edge needs less phase delay. Thus, the phase distributions of Ant III are more uniform than those of Ant II at 1.15, 5, 8, and 12 GHz, as shown in Fig. 7.

III. MEASURED RESULTS AND DISCUSSION

In order to verify the proposed approach, the designed Ant III was fabricated, as shown in Fig. 14. The circuit was measured using a Keysight ENA E5071C Network Analyzer in an anechoic environment. The measured S_{11} of the designed Ant III is illustrated in Fig. 15 and compared with the simulated data. S_{11} of Ant III is better than –10 dB over the frequency band of 1.13–12 GHz. It is slightly worse at 2.06–2.27 GHz but still better than –9.3 dB. In the operating frequency band of 1.13–12 GHz, the measured gain of the designed Ant III varies in the range of 0.7–14 dBi, as shown in Fig. 16. The main reason for the difference between the measurement and the simulation is that the radiation surface of the fabricated antenna has slight wear and bend.

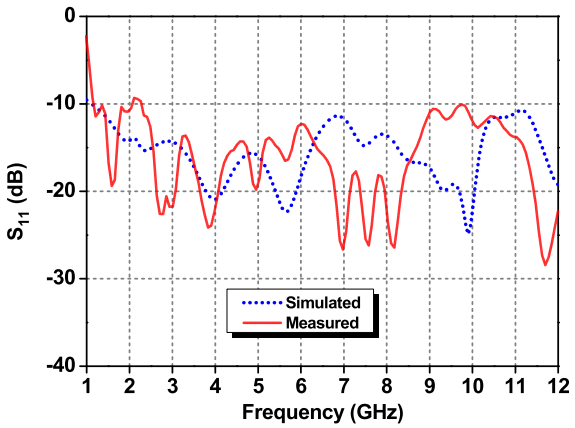

FIGURE 15. Comparison of simulated and measured S_{11} for the proposed Ant III.

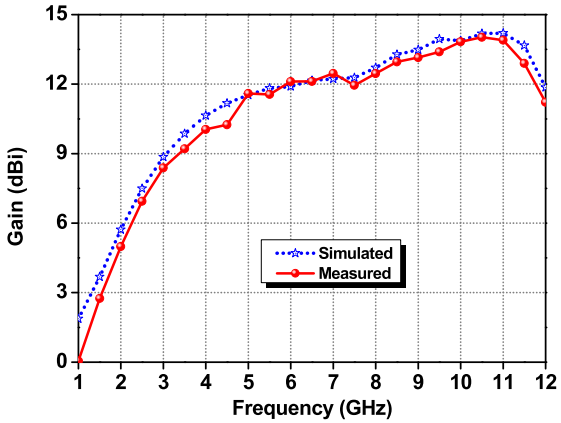

FIGURE 16. Comparison of simulated and measured gains for the proposed Ant III.

TABLE 2. Comparison of the proposed Ant III to other Vivaldi antenna literatures.

Ref. No.	Operating frequency (GHz)	Size ($\lambda_g \times \lambda_g \times \lambda_g$)	Max gain (dB)	
			Simulated	Measured
[7]	3–15.1	0.79 × 0.67 × 0.013	8.5	8.2
[8]	5–50	1.36 × 0.74 × 0.013	14	N.M
[10]	2–12	0.61 × 0.55 × 0.009	N.M	12.4
[11]	1.32–17	0.56 × 0.54 × 0.005	N.M	9.3
[12]	2.4–14	1.16 × 0.92 × 0.019	N.M	10
[13]	3.4–40	1.51 × 0.67 × 0.009	15	N.M
[15]	5–27	3.28 × 1.54 × 0.036	12.2	N.M
This work	1.13–12	0.76 × 0.41 × 0.005	14.2	14

N.M states the not mentioned, λ_g is the guided wavelength at the lowest frequency of the resonant band.

To clearly illustrate the performance of the proposed antenna, simulated and measured normalized radiation patterns of Ant III at 1.15 GHz, 5 GHz, 8 GHz and 12 GHz are plotted in Fig. 17. As can be observed, the half-power beamwidth is wider with lower directivity at low frequencies, while at the high frequencies, the half-power beamwidth is narrower with higher directivity. Additionally, the cross-polarizations of Ant III in the E-plane and H-plane are also shown in Fig. 17. The measured cross-polarizations of Ant III behave well and maintained as –27 dB at 1.15 GHz, –25 dB at 5 GHz, –20 dB at 8 GHz, and –18 dB at 12 GHz in both E- and H-planes at the axial direction. A further proof to demonstrate the higher gain is given by adding the radiation patterns of Ant II, as shown in Fig. 18. As it can be observed, the simulated half-power beamwidth of Ant II is 103.2° at 1.15 GHz, 45.1° at 5 GHz, 27.4° at 8 GHz, 22.6° at 12 GHz in E-plane, and 219.1° at 1.15 GHz, 87.3° at 5 GHz, 48.8° at 8 GHz, 41.8° at 12 GHz in H-plane. For Ant III, the simulated half-power beamwidth is 103.2° at 1.15 GHz, 45.1° at 5 GHz, 32.4° at 8 GHz, 22.6° at 12 GHz in E-plane, and 219.1° at

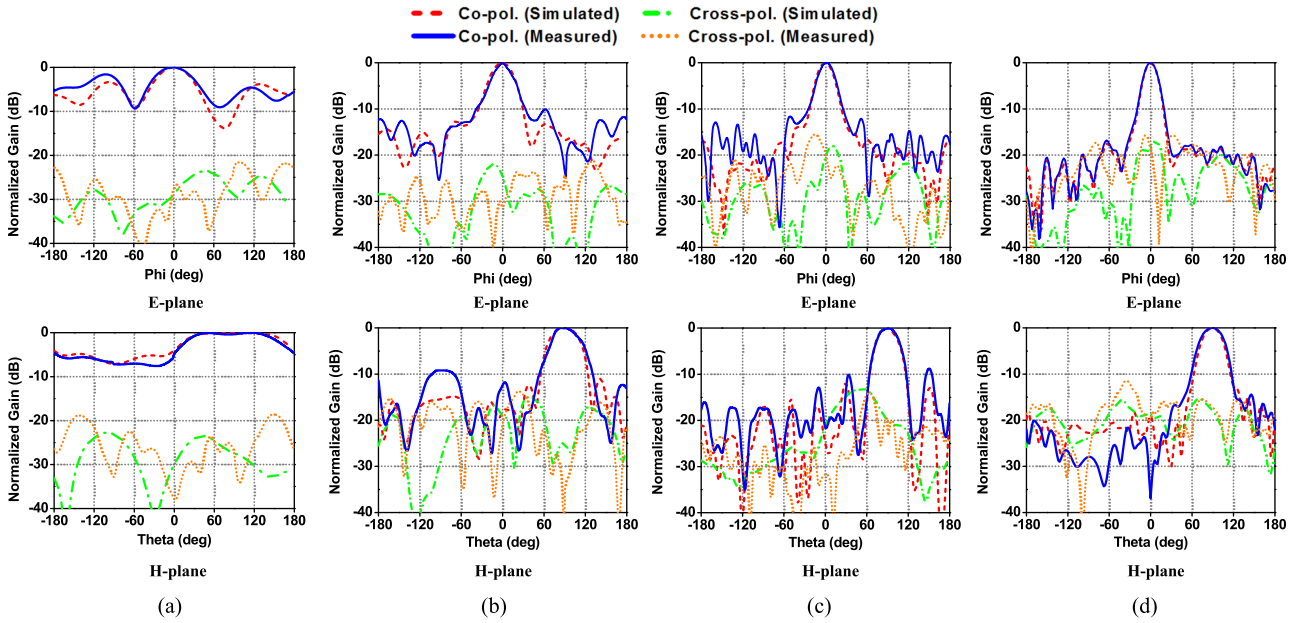

FIGURE 17. Simulated and measured E- and H-plane radiation patterns of the proposed Ant III at (a) 1.15 GHz, (b) 5 GHz, (c) 8 GHz and (d) 12 GHz.

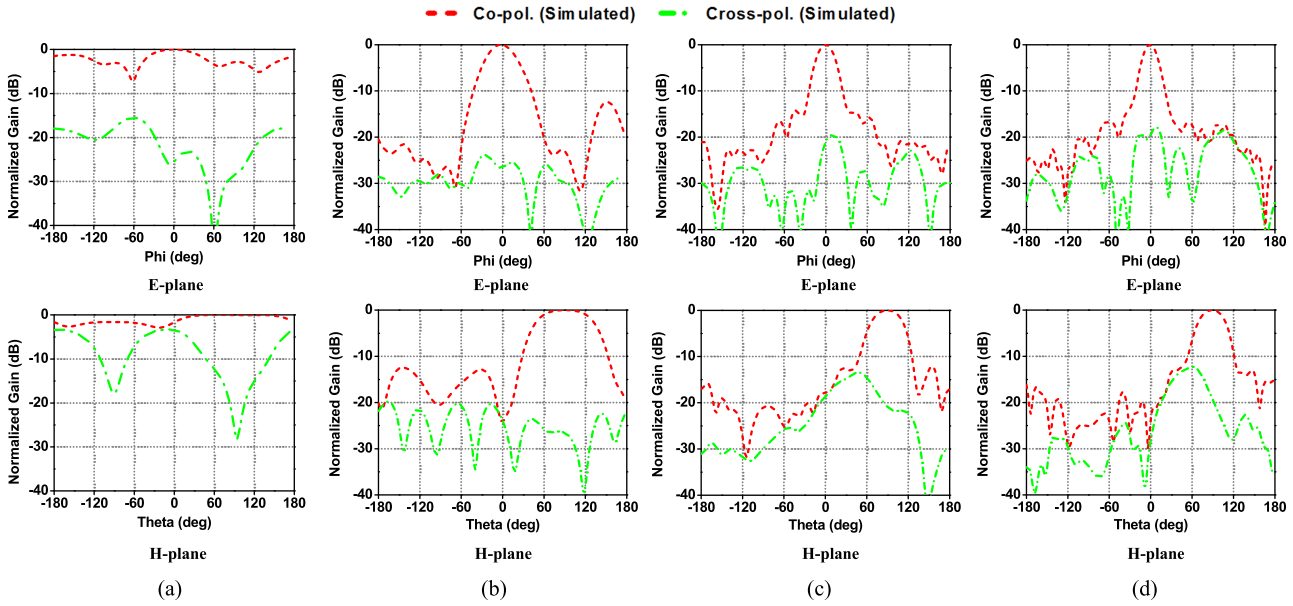

FIGURE 18. Simulated E- and H-plane radiation patterns of Ant II at (a) 1.15 GHz, (b) 5 GHz, (c) 8 GHz and (d) 12 GHz.

1.15 GHz, 87.3° at 5 GHz, 56.7° at 8 GHz, 41.8° at 12 GHz in H-plane. The half-power beamwidth of Ant II is wider than that of Ant III.

Table 3 compares the proposed Ant III with other Vivaldi antennas mentioned in Section I. As can be seen from Table 3 that the proposed Ant III offer comparable and even better performance in terms of dimension and gain.

IV. CONCLUSION

A miniaturized DSVA with a fractional bandwidth of 169% from 1.15 to 12 GHz and a directional radiation pattern has presented in this paper. A pair of defected ground slots are developed to extend the low cut-off frequency from 2.27 GHz to 1.15 GHz. In order to improve the gain in the wide frequency band, an MS is inserted into the slot of the proposed DSVA. The designed MS consists of 2×8 two-stub-loaded SRR elements along the x- and y-directions, respectively. As expected, the proposed antenna has a high gain of 2.27–11.9 dB from 1.11 to 6 GHz in comparison with the antenna without MS, whose gain is from 1.11 to 11.42 dBi in the range of 1.15–6 GHz. In the higher frequency band of 9–12 GHz, the proposed MS introduces conductor loss and

it contributes to a gain decrease of 0.06–0.32 dBi compare to that without MS. Finally, the proposed antenna has been fabricated and measured to verify the proposed design method.

REFERENCES

[1] P. J. Gibson, "The Vivaldi aerial," in *Proc. 9th Eur. Microw. Conf.*, Sep. 1979, pp. 101–105.

[2] L. Wang, "Early diagnosis of breast cancer," *Sensors*, vol. 17, no. 7, pp. 1–20, Jul. 2017.

[3] J. Yan, H. Hong, H. Zhao, Y. Li, C. Gu, and X. Zhu, "Through-wall multiple targets vital signs tracking based on VMD algorithm," *Sensors*, vol. 16, no. 8, pp. 1293–1303, Aug. 2016.

[4] M. Martín-Neira *et al.*, "Microwave interferometric radiometry in remote sensing: An invited historical review," *Radio Sci.*, vol. 49, no. 6, pp. 415–449, 2014.

[5] X. Zhuge and A. G. Yarovoy, "A sparse aperture MIMO-SAR-based UWB imaging system for concealed weapon detection," *IEEE Trans. Geosci. Remote Sens.*, vol. 49, no. 1, pp. 509–518, Jan. 2011.

[6] J.-P. Hsu, T. Hiraoka, and Y. Tabei, "Analysis of stripline right-angle bend with slant-wise corner cut based on Eigenmode expansion method and Foster-type equivalent network," in *IEEE MTT-S Int. Microw. Symp. Dig.*, Anaheim, CA, USA, Jun. 1999, pp. 1315–1318.

[7] J. Wu, Z. Zhao, Z. Nie, and Q.-H. Liu, "A printed UWB Vivaldi antenna using stepped connection structure between slotline and tapered patches," *IEEE Antennas Wireless Propag. Lett.*, vol. 13, pp. 698–701, 2014.

[8] M. Moosazadeh, S. Kharkovsky, J. T. Case, and B. Samali, "Improved radiation characteristics of small antipodal Vivaldi antenna for microwave and millimeter-wave imaging applications," *IEEE Antennas Wireless Propag. Lett.*, vol. 16, pp. 1961–1964, 2017.

[9] E. W. Reid, L. Ortiz-Balbuena, A. Ghadiri, and K. Moez, "A 324-element Vivaldi antenna array for radio astronomy instrumentation," *IEEE Trans. Instrum. Meas.*, vol. 61, no. 1, pp. 241–250, Jan. 2012.

[10] G. K. Pandey, H. Verma, and M. K. Meshram, "Compact antipodal Vivaldi antenna for UWB applications," *Electron. Lett.*, vol. 51, no. 4, pp. 308–310, 2015.

[11] Z. Wang, Y. Yin, J. Wu, and R. Lian, "A miniaturized CPW-fed antipodal Vivaldi antenna with enhanced radiation performance for wideband applications," *IEEE Antennas Wireless Propag. Lett.*, vol. 15, pp. 16–19, 2016.

[12] P. Fei, Y.-C. Jiao, W. Hu, and F.-S. Zhang, "A miniaturized antipodal Vivaldi antenna with improved radiation characteristics," *IEEE Antennas Wireless Propag. Lett.*, vol. 10, pp. 127–130, 2011.

[13] M. Moosazadeh and S. Kharkovsky, "A compact high-gain and front-to-back ratio elliptically tapered antipodal Vivaldi antenna with trapezoid-shaped dielectric lens," *IEEE Antennas Wireless Propag. Lett.*, vol. 15, pp. 552–555, 2016.

[14] J. Bourqui, M. Okoniewski, and E. C. Fear, "Balanced antipodal Vivaldi antenna with dielectric director for near-field microwave imaging," *IEEE Trans. Antennas Propag.*, vol. 58, no. 7, pp. 2318–2326, Jul. 2010.

[15] I. T. Nassar and T. M. Weller, "A novel method for improving antipodal Vivaldi antenna performance," *IEEE Trans. Antenna Propag.*, vol. 63, no. 7, pp. 3321–3324, Jul. 2015.

[16] R. W. Ziolkowski, P. Jin, and C.-C. Lin, "Metamaterial-inspired engineering of antennas," *Proc. IEEE*, vol. 99, no. 10, pp. 1720–1731, Oct. 2011.

[17] S. Chaimool, C. Rakluea, and P. Akkaraekthalin, "Mu-near-zero metasurface for microstrip-fed slot antennas," *Appl. Phys. A, Solids Surf.*, vol. 112, no. 3, pp. 669–675, 2013.

[18] M. Memarian and G. V. Eleftheriades, "Dirac leaky-wave antennas for continuous beam scanning from photonic crystals," *Nature Commun.*, vol. 6, Jan. 2015, Art. no. 5855.

[19] B. Zhou and T. J. Cui, "Directivity enhancement to Vivaldi antennas using compactly anisotropic zero-index metamaterials," *IEEE Antennas Wireless Propag. Lett.*, vol. 10, pp. 326–329, 2011.

[20] M. Sun, Z. N. Chen, and X. Qing, "Gain enhancement of 60-GHz antipodal tapered slot antenna using zero-index metamaterial," *IEEE Trans. Antennas Propag.*, vol. 61, no. 4, pp. 1741–1746, Apr. 2013.

[21] Y.-W. Wang, G.-M. Wang, and B.-F. Zong, "Directivity improvement of Vivaldi antenna using double-slot structure," *IEEE Antennas Wireless Propag. Lett.*, vol. 12, pp. 1380–1383, 2013.

[22] P. Kumar, Z. Akhter, A. K. Jha, and M. J. Akhtar, "Directivity enhancement of double slot Vivaldi antenna using anisotropic zero-index metamaterials," in *Proc. IEEE Int. Symp. Antennas Propag.*, Jul. 2015, pp. 2333–2334.

[23] R. W. P. King, *Transmission-Line Theory*. New York, NY, USA: McGraw-Hill, 1955, ch. 5, pp. 288–317.

[24] B. C. Wadell, *Transmission Line Design Handbook*. Norwood, MA, USA: Artech House, 1991.

[25] J. Bai, S. Shi, and D. W. Prather, "Modified compact antipodal Vivaldi antenna for 4–50-GHz UWB application," *IEEE Trans. Microw. Theory Techn.*, vol. 59, no. 4, pp. 1051–1057, Apr. 2011.

[26] D. R. Smith, D. C. Vier, T. Koschny, and C. M. Soukoulis, "Electromagnetic parameter retrieval from inhomogeneous metamaterials," *Phys. Rev. E, Stat. Phys. Plasmas Fluids Relat. Interdiscip. Top.*, vol. 71, pp. 036617-1–036617-11, Mar. 2005.

[27] G. K. Pandey and M. K. Meshram, "Anisotropic artificial material with ENZ and high refractive index property for high gain Vivaldi antenna design," in *Proc. IEEE Medit. Microw. Symp. (MMS)*, Nov./Dec. 2015, pp. 1–4.

[28] R. Halir *et al.*, "Recent advances in silicon waveguide devices using subwavelength gratings," *IEEE J. Sel. Topics Quantum Electron.*, vol. 20, no. 4, Jul./Aug. 2014, Art. no. 8201313.

[29] Z. Tao, W. X. Jiang, H. F. Ma, and T. J. Cui, "High-gain and high-efficiency GRIN metamaterial lens antenna with uniform amplitude and phase distributions on aperture," *IEEE Trans. Antennas Propag.*, vol. 66, no. 1, pp. 16–22, Jan. 2018.

SHUANGSHUANG ZHU (S'16) was born in Henan, China, in 1991. She received the B.S. degree in electronic engineering from the North China University of Water Resources and Electric Power, Zhengzhou, China, in 2012, and the M.S. degree in communication and information system from East China Jiaotong University, Nanchang, China, in 2015. She is currently pursuing the Ph.D. degree with the School of Electronic and Information Engineering, Xi'an Jiaotong University, Xi'an, China.

Her current research interests include antenna array, millimeter-wave antenna, and metasurface.

HAIWEN LIU (M'04–SM'13) received the B.S. degree in electronic system and the M.S. degree in radio physics from Wuhan University, Wuhan, China, in1997 and 2000, respectively, and the Ph.D. degree in microwave engineering from Shanghai Jiao Tong University, Shanghai, China, in 2004. From 2004 to 2006, he was with Waseda University, Kitakyushu, Japan, as a Research Assistant Professor. From 2006 to 2007, he was a Research Fellow with Kiel University, Kiel, Germany, where he was granted the Alexandervon Humboldt Research Fellowship. From 2007 to 2008, he was a Professor with the Institute of Optics and Electronics, Chengdu, China, where he was supported by the 100 Talents Program of Chinese Academy of Sciences. Since 2009, he has been a Chair Professor with East China Jiaotong University, Nanchang, China. He has published more than 100 papers in international and domestic journals and conferences. His current research interests include electromagnetic modeling of high-temperature superconducting circuits, radio frequency and microwave passive circuits and systems, antennas theory, and radar system.

Dr. Liu has served as a Technical Program Committee Member for many international conferences and a reviewer for some international journals, including the IEEE Transactions on Microwave Theory and Technique, the IEEE Transactions on Applied Superconductivity, the IEEE Transactions on Industrial Electronics, the IEEE Microwave and Wireless Components Letters, and the IEEE Antennas and Wireless Propagation Letters. He was a recipient of the Best Paper Prize of the 2005 International Conference on Communications, Circuits and Systems Proceedings in Hong Kong, the Prize of Osaka City Mayor for Conference of Chinese Alumni in Japan in 2005, the 100 Best Ph.D. Dissertations in Shanghai, China, in 2006,and Wang Kuancheng Science Foundation in 2008.

PIN WEN (S'16) received the B.S. degree in communication engineering and the M.S. degree in communication and information system from East China Jiaotong University, Nanchang, China, in 2012 and 2015, respectively. He is currently pursuing the Ph.D. degree in microwave engineering with Xi'an Jiaotong University, China.

In 2015, he became a Research Assistant with East China Jiaotong University. His current research interests include antenna theory and design, and superconducting filter design.

LIXIA DU received the M.S. degree in communication and information system from East China Jiaotong University, Nanchang, China, in 2015.

Her current research interests include antenna theory and design.

JIAFENG ZHOU received the B.Sc. degree in radio physics from Nanjing University, Nanjing, China, in 1997, and the Ph.D. degree from the University of Birmingham, Birmingham, U.K., in 2004. His doctoral research concerned high-temperature superconductor microwave filters.

From 1997 to 1999, he was with the National Meteorological Satellite Center, Beijing, China, where he was involved in the development of communication systems for Chinese geostationary meteorological satellites. From 2004 to 2006, he was a Research Fellow with the University of Birmingham, where his research concerned phased arrays for reflector observing systems. He then joined the Department of Electronic and Electrical Engineering, University of Bristol, Bristol, U.K., where he remained until 2013. His research with the University of Bristol concerned the development of highly efficient and linear amplifiers. He is currently with the Department of Electrical Engineering and Electronics, University of Liverpool, Liverpool, U.K. His current research interests include microwave power amplifiers, filters, electromagnetic energy harvesting, and wireless power transfer.